IEEE Open Journal of Power Electronics

Received XX Month, XXXX; revised XX Month, XXXX; accepted XX Month, XXXX; Date of publication XX Month, XXXX; date of current version XX Month, XXXX.

Digital Object Identifier 10.1109/OJPEL.XXXX.XXXXXX

Impact of the Converter Controller on Power Hardware-in-the-Loop Testing Stability and Accuracy

FARGAH ASHRAFIDEHKORDI [1] (Member, IEEE), GIAMPAOLO BUTICCHI [2] (Senior Member, IEEE), PANOS KOTSAMPOPOULOS [3] (Senior Member, IEEE), AND GIOVANNI DE CARNE [1] (Senior Member, IEEE)

[1]Institute for Technical Physics, Karlsruhe Institute of Technology, Karlsruhe 76344, Germany
[2]Key Laboratory of More Electric Aircraft Technology of Zhejiang Province, University of Nottingham Ningbo China, Ningbo 315100, China
[3]School of Electrical and Computer Engineering, National Technical University of Athens, Greece

CORRESPONDING AUTHOR: GIOVANNI DE CARNE (e-mail: giovanni.carne@kit.edu).

Their work has been supported by the Helmholtz Association under the program "Energy System Design" and under the Helmholtz Young Investigator Group "Hybrid Networks" (VH-NG-1613)

ABSTRACT Power electronics play a crucial role in integrating renewable energy sources into modern power systems. To ensure their reliable deployment, advanced testing methods such as Power Hardware-in-the-Loop (PHIL) are essential for evaluating their behavior under realistic grid conditions. This paper investigates the impact of the Hardware of Interest (HoI)—a three-phase grid-following DC/AC converter—on the stability and accuracy of PHIL setups. A loop-based transfer function model is developed to represent the PHIL system, including the HoI dynamics, power interface, and real-time simulator. Using this model, a sensitivity analysis is performed to examine how the converter's control parameters—particularly the current controller bandwidth—affect PHIL stability and accuracy. Perturbation-based frequency-domain scans are conducted in MATLAB/Simulink and experimentally validated on a 45 kVA PHIL platform.

INDEX TERMS Power Hardware-in-the-loop, power electronics testing, stability analysis, accuracy analysis, grid-connected converter.

I. INTRODUCTION

NEW energy technologies are currently being developed to accelerate the transition toward low-emission energy systems across production, transportation, and utility sectors. Particular attention has been given to power electronics-based systems, such as energy storage systems, electric vehicles, and renewable energy sources. These technologies typically share a power electronics interface with the power grid that guarantees maximum power extraction, higher energy efficiency, and offer grid services [1].

Despite significant industrial efforts to bring these technologies to the market, the industry encounters a bottleneck when it comes to experimental validation before commercial deployment. Even though a reliable testing approach, e.g., actual field testing, is considered quite accurate and with high result fidelity, it requires a significant amount of time and resources to explore all the possible grid conditions that the technology may encounter during operations [2]. Additionally, adopting technologies in a power grid that have not yet been thoroughly tested raises concerns among grid operators about potential disruptions to regular service [3].

To address this issue and support faster deployment, the Power Hardware-in-the-Loop (PHIL) testing approach allows interfacing the Hardware-of-Interest (HoI), e.g., from commercial loads to power electronic converters or entire grids, with a real-time simulated network through a power interface [4]–[6]. As shown in Fig. 1(a), the idea of PHIL is to enable the interaction between the real-world power equipment, i.e., HoI, and the simulated Model-of-Interest (MoI) in the real-time simulator. In Fig. 1(b), the required interfaces for integrating the HoI to the MoI are illustrated. The digital-to-analog (D/A) and analog-to-digital (A/D) converters are responsible for translating the output signals of the Digital Real-Time Simulator (DRTS) into analog signals

This work is licensed under a Creative Commons Attribution 4.0 License. For more information, see https://creativecommons.org/licenses/by/4.0/

for the real-life HoI and for converting measured analog signals from the HoI back into digital form for the simulator. A power amplifier is used to transform the simulator's output signals into real power suitable for operating the power hardware. Sensors measure electrical variables at the HoI and send them back to the MoI in the DRTS to complete the dynamic interaction between HoI and MoI. A low-pass filter, although optional, is commonly included to reject high-frequency measurement noise and enhance the stability of the PHIL setup. Therefore, a PHIL is able to emulate various grid scenarios in a simulation environment, e.g., day-night, winter-summer power profiles, and evaluating the real-life HoI response to these scenarios. As a result, it drastically shortens the development time and allows for preliminary validation in a controlled environment before transferring the HoI to the target systems. Large-scale examples [7], [8] show the advantages of testing real devices in a safe and flexible setting.

However, it is well known that PHIL testing faces stability challenges due to the introduction of components not present in the actual field, such as power amplifiers, data converters, and filtering stages. Although many studies have addressed PHIL stability and accuracy challenges, the HoI is still commonly represented as a passive impedance [5], [6], [9], [10], making the current PHIL applications unrealistic.

In [11], a novel interface technique has been proposed for increasing stability during PHIL testing for power electronics; however, the power converter has been represented only as a passive transfer function without including the controller's influence. In this way, the dynamics of the power electronics connected to the loop are ignored, and this could lead to an overestimation of the loop stability or a loss of testing fidelity. Recently, some papers have started to include power electronics converter dynamics in the stability and accuracy analysis of PHIL setups. For example, in [12], the inverter's control and delays are included in the PHIL stability assessment, using the well-known impedance stability analysis to understand the stability boundaries under variable emulated grid and hardware impedances. In [13], it is revealed how the converter's control can lead to a misleading interpretation of the Nyquist criterion when employing impedance-based stability analysis. In [14], the impact of asymmetries in Low-Voltage Ride-Through testing for power converters on the PHIL accuracy has been studied.

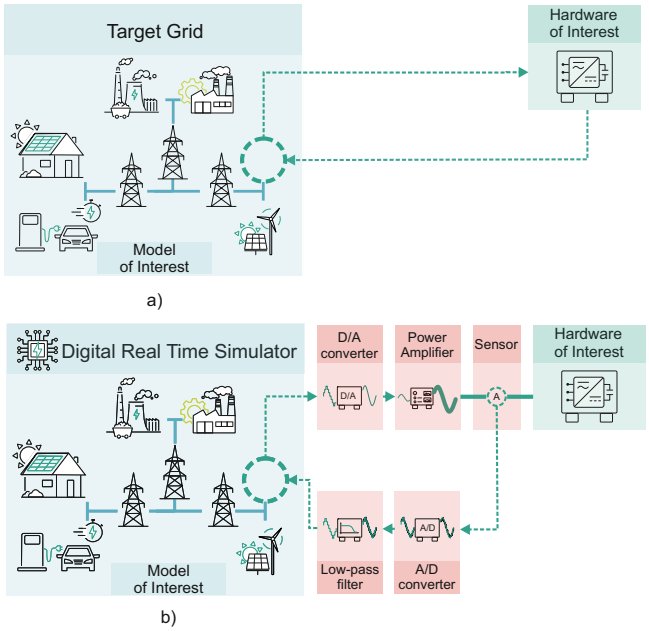

FIGURE 1. Power Hardware-in-the-Loop concept: a) Natural coupling b) Power Hardware-in-the-Loop coupling.

However, a study on the impact of power electronic converters on PHIL stability and accuracy has not been performed yet. Varying the power converter controller bandwidth, the equivalent transfer function of the power converter changes, shifting the stability boundaries of the PHIL testing. For this reason, this paper introduces a novel mathematical approach that analyzes the impact on the PHIL stability and accuracy of a three-phase current-controlled voltage-source converter as the HoI. The contributions of this paper can be summarized as follows:

- Dynamic behavior comparison of the proposed approach, including the converter's controller, with classical approaches, including only the passive elements in the analysis.
- The impact of the converter controller's bandwidth on the accuracy and the stability of the PHIL results
- Parameter sensitivity analysis of the current controller bandwidth, different loop filters, and simulated impedances.
- Experimental validation of the PHIL and HoI modeling with the 45 kVA PHIL setup and a three-phase power converter with digital controller.

The paper is organized as follows: Section II reviews state-of-the-art, Section III describes how to mathematically model the PHIL system, Section IV verifies the modeled PHIL and HoI with Simulations, Section V shows how the HoI impacts the PHIL system, Section VI analyzes how the low-pass filter in the feedback affects the system performance, Section VII shows similar analysis with different grid-impedances, Section VIII, presents the experimental verification of the modeling, and Section IX draws the conclusion.

This article has been accepted for publication in IEEE Open Journal of Power Electronics. This is the author's version which has not been fully edited and content may change prior to final publication. Citation information: DOI 10.1109/OJPEL.2025.3623169

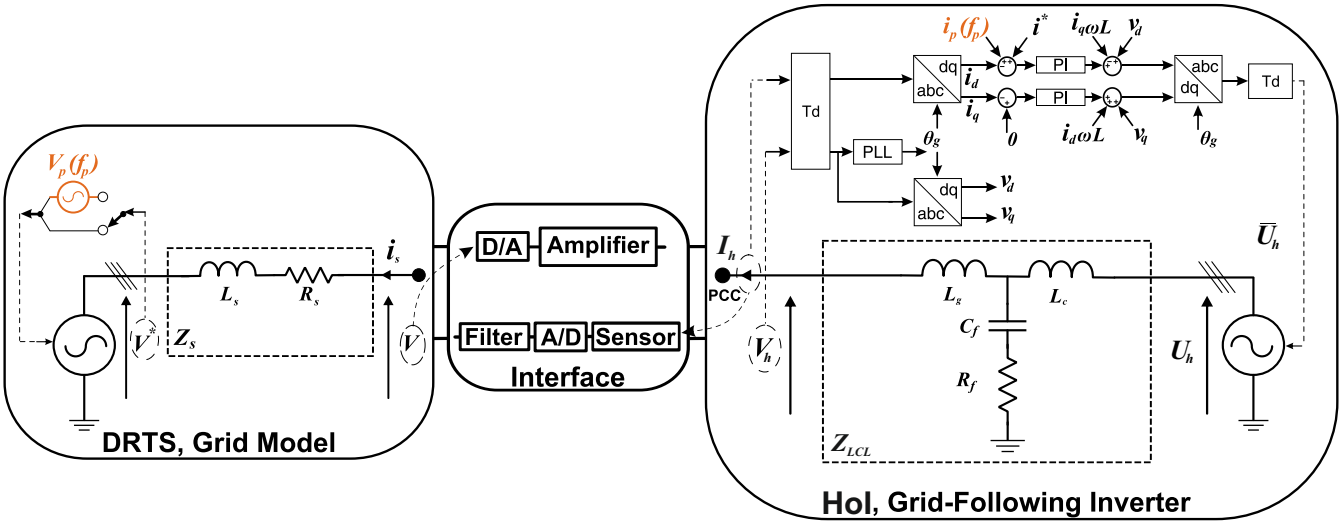

FIGURE 2. **Power Hardware-in-the-Loop setup with 3 phase DC/AC converter as Hardware-of-Interest.**

II. STATE-OF-THE-ART ON PHIL

Concerning the natural coupling scheme (Fig. 1(a)), which represents the ideal case when the HoI is directly connected with a real grid, the PHIL testing results may deviate from this ideal behavior due to the presence of interface components. These interfaces can introduce inaccuracies, potentially compromising the validity of the test results [23]. In addition to inaccuracy, it is highlighted in the literature that the time delay introduced by the power amplifier, the simulator, and the current/voltage sensors can eventually cause instability in the PHIL system [15]. Hence, the stability analysis for PHIL testing has also been the subject of intensive investigation in recent years, as reviewed in the well-known literature [5], [6], [24]. Several interface algorithms, such as the Ideal Transformer Method (ITM), Partial Circuit Duplication (PCD), Damping Impedance Method (DIM), and Transmission-line Method (TLM), to connect the MoI to the HoI are evaluated in [10] to improve the stability and accuracy of a PHIL, among which the ITM is regarded as a straightforward and accurate algorithm. However, when the ITM is used, the stability of the PHIL setup is limited to the software/hardware impedance-ratio criterion. Another interface algorithm with a better stability margin than ITM is the DIM, which combines ITM with the PCD. In [25], [26], the wideband system identification technique is employed to enhance the DIM interface algorithm, thereby ensuring simulation stability and accuracy. The modified DIM is proposed in [27], which updates the linking impedance parameters with a new value of the load under test. Due to the added complexity and implementation costs of the DIM, the ITM—and its variants—have been further modified to maintain simplicity while enhancing the stability of PHIL. For example, the use of a feedback filter in ITM is one of the most common techniques to ensure PHIL stability in a large set of testing conditions. As shown in Fig. 1(b), the concept of this method is to add a low-pass filter in the feedback loop in the DRTS software. This approach, firstly proposed in [28], allows for dampening the system dynamics and thus strengthening the stability of the PHIL loop. The main advantage of this method lies in its implementation simplicity, as the low-pass filter can be easily applied in the simulated part as a transfer function inside the DRTS. Additional work has considered network compensators based on feedback transfer functions to stabilize the PHIL in a larger set of operative conditions [29]. Although stability can be significantly improved, the use of low-pass filters or compensators impacts the phase and the magnitude of the PHIL transfer function, consequently impacting, the accuracy of the testing with respect to the natural coupling. The accuracy of PHIL testing has been a subject of ongoing discussion for years. In [30], several indexes based on amplitude and phase difference have been introduced in order to validate mathematical models and the PHIL testing concerning the natural coupling of the system. However, it focuses exclusively on passive loads (linear and non-linear) without providing any realistic approach for assessing the accuracy of power electronics converter testing. The discrete-time impedance frequency responses are preferred for better evaluating PHIL stability over conventional continuous-time-based analysis [31], as PHIL is not a fully continuous system. It has been demonstrated that hybrid continuous and discrete modeling approaches are needed for more accurate modeling of the PHIL testing [32].

Recent contributions have extended PHIL applications to power converters as HoI, focusing on improving both feasibility and stability. The approaches in [20] and [33] introduce physics-informed and harmonic-invariant scaling techniques, respectively, to replicate the behavior of full-scale converters using smaller hardware. A reinforcement learning-based interface control strategy is introduced in [16] to handle uncertain system dynamics. The work in [22] proposes a multirate co-simulation framework for large-

TABLE 1. A SELECTION OF State-Of-The-Art On PHIL TESTING

Reference(s)	Interface Algorithm	Stability Analysis	PHIL Accuracy Across Frequency Range	Active HoI	HoI Impact On the Accuracy of PHIL
[15]	ITM	✓	✗	✗	✗
[16]	ADP-based[1] & HI[2]	✓	✗	✓	✗
[17]	ITM with SP[3]	✓	✗	✓	✗
[18]	multi-dimentional GSS-based[4]	✓	✗	✓	✗
[19]	μ-synthesis-based	✓	✗	✓	✗
[8], [14], [20]	ITM	✗	✗	✓	✗
[21]	ITM	✓	✗	✓	✗
[22]	Modified ITM	✓	✗	✓	✗
[12]	ITM	✓	✗	✓	✗
This article	ITM + Low-Pass Filter	✓	✓	✓	✓

[1] ADP: Adaptive Dynamic Programming
[2] HI: Hybrid Iteration
[3] SP: Smith Predictor
[4] GSS: Golden Section Search

scale PHIL applications. Additionally, [18] presents a novel power interface using a golden section search algorithm to relax impedance ratio constraints. [17] implements a Smith predictor to mitigate delay-induced instability, and [19] applies μ-synthesis—a robust control method—to design PHIL interface controllers under model uncertainties. Authors in [21] study RHP poles in PHIL with a grid-tied converter using D–Q impedance modeling and link their emergence to PLL dynamics.

As shown in the Table 1, the majority of these works focus on interface algorithms improvements, with the ITM still being widely used due to its simplicity. However, these studies generally assess accuracy in the time domain or by comparing different interface algorithms—rather than benchmarking against an ideal natural coupling. Furthermore, the HoI is not explicitly analyzed as a possible source of inaccuracy. To the best of the author's knowledge, no prior work has investigated how the internal dynamics of an active HoI—such as a grid-following converter—affect the accuracy of PHIL testing. This work addresses this overlooked aspect by analyzing the impact of the HoI's current controller bandwidth on both stability and frequency-domain accuracy, offering new insights into how HoI control dynamics influence PHIL performance beyond the interface sector. To demonstrate this impact, a voltage-type ITM (V-ITM) with a linear power amplifier and a low-pass filter in the feedback loop is employed as a PHIL benchmark when the HoI is a three-phase DC/AC grid converter. Accuracy is studied by comparing the PHIL with the natural coupling frequency responses, and stability is analyzed using pole-zero maps, first by modeling each component and then the entire PHIL via transfer functions in the discrete domain. The main contribution of this work is to investigate the impact of the converter current controller bandwidth not only on stability but also on the accuracy of the PHIL. Also, the obtained transfer functions are verified via simulations and experiments.

III. MATHEMATICAL FORMULATION OF THE SELECTED PHIL SETUP

This section aims to introduce the mathematical modelling of the benchmark PHIL, namely the grid model, interfaces, and the grid-connected converter with and without its controller, versus the natural coupling case.

A. GRID-CONNECTED CONVERTER MODEL

The ideal case of a converter directly connected to a distribution grid shall be analyzed first to represent the natural coupling case. The Thevenin equivalent circuit is used for the grid model as shown in Fig. 2, where the grid is represented by a voltage source V^* and line impedance $Z_s = R_s + j\omega L_s$. The converter is represented with an average model, composed of a voltage source U_h and the filter LCL impedance [34]. The perturbation sources, shown in orange, are implemented to excite the system at both sides of the PCC over a wide frequency range, which will be used in the next section, where the transfer functions achieved in this section are verified. The transfer function of the system shown in Fig. 2 is illustrated in Fig. 3, and described mathematically as:

$$\frac{I_h(z)}{I^*(z)} = \frac{C(z)Y(z)z^{-1}}{1 + C(z)Y(z)z^{-2}} \tag{1}$$

where $C(z)$ and $Y(z)$ represent the proportional-integral controller and the combined admittance of the converter and the grid, respectively:

$$C(z) = Z\{K_p(1+\frac{1}{s})\} = K_p(1+K_iT_s\frac{1}{(z-1)}) \quad (2)$$

$$\begin{aligned} Y(z) &= Y_h(z) + Y_s(z) \\ Y_h(z) &= Z\{\frac{sC_fR_f+1}{As^3+Bs^2+Cs+D}\} \\ Y_s(z) &= Z\{\frac{1}{R_s+L_ss}\} = \frac{1+z^{-1}}{R_s+2\frac{L_s}{T_s}+(R_s-2\frac{L_s}{T_s})z^{-1}} \end{aligned} \quad (3)$$

Where the LCL formulation can be expanded as [35]:

$$\begin{aligned} A =& C_fL_cL_g \\ B =& C_fL_cR_f + C_fL_gR_f + C_fL_cR_g + C_fL_gR_c \\ C =& L_c + L_g + C_fR_fR_c + C_fR_fR_g + C_fR_cR_g \\ D =& R_c + R_g \end{aligned} \quad (4)$$

The following assumption has been made to perform the analysis in the discrete domain:

- The discretization of these variables has been performed using the Tustin method with a time sampling equal to $Ts = 50\,\mu$s.
- The PWM and measurement delays in the converter have been assumed to be equal to T_s to simplify the PHIL mathematical analysis. While different delays, converter types, or control strategies may yield varying numerical results, the proposed modeling framework remains valid and applicable.

B. PHIL MODEL FOR STABILITY EVALUATION

The classical approach to evaluate the PHIL system stability is to consider the HoI with its equivalent passive impedance (e.g., the AC filter of a converter), as shown in Fig. 3(a). The equivalent closed-loop transfer function can be expressed mathematically as:

$$\frac{I_h(z)}{V^*(z)} = \frac{PA(z)Y_h(z)z^{-1}}{1+F(z)PA(z)\frac{Y_h(z)}{Y_s(z)}z^{-2}} \quad (5)$$

Where the filter transfer function consists of a low-pass filter with time constant T_f:

$$F(z) = Z\{\frac{1}{1+T_fs}\} = \frac{(1+z^{-1})\frac{T_s}{T_s+2T_f}}{(1+z^{-1})\frac{T_s-2T_f}{T_s+2T_f}} \quad (6)$$

It is assumed that the power amplifier has a unity gain $PA(z) = 1$. This assumption is correct if the transient response of the amplifier is faster than the simulator time step $T_s = 50\,\mu$s. In the case of linear power amplifiers, their fast voltage slew rate allows them to reach the new steady state condition in about $4\,\mu$s, more than ten times smaller than T_s.

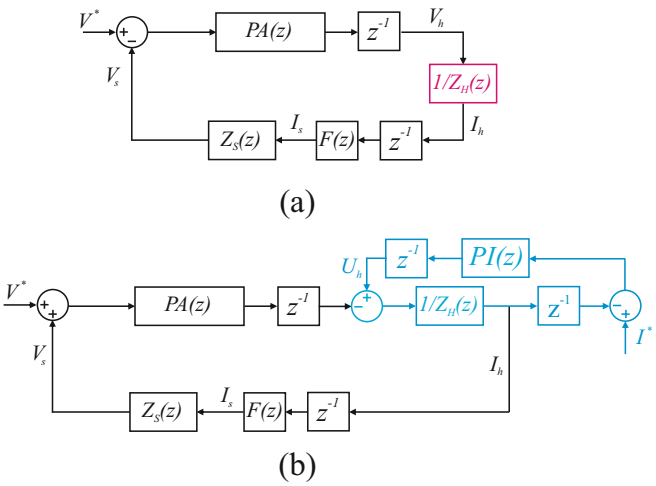

FIGURE 3. PHIL block diagram: a) without controller loop b) with controller loop.

Following this modelling, the stability is determined by the impedance ratio $\frac{Y_h(z)}{Y_s(z)}$. If this ratio satisfies the Nyquist criterion, the stability is guaranteed. If not, the system is not stable, and corrective actions must be taken to guarantee the stability.

However, as can be noted from the mathematical formulation in (5), the controller of the converter is not taken into account during the analysis. As demonstrated in the next section, this leads to a wrong characterization of the system frequency behavior and, thus, of its stability.

C. PHIL MODEL CONSIDERING THE CONVERTER CONTROL

This section introduces the PHIL model, which includes a simplified converter model in the PHIL mathematical representation. The red-marked part shown in Fig. 3(a) is now substituted with the blue-marked part in Fig. 3(b). It includes the AC filter impedance $1/Y_h(z)$ and the converter controller $C(z)$:

$$C(z) = K_p(1+\frac{K_iT_s}{z-1}) \quad (7)$$

The main difference between the two figures is that while the AC filter remains in the forward path, the controller $C(z)$ provides a feedback action for the loop.

The internal loop of the converter, $CC_{loop}(z)$, can be described as:

$$CC_{loop}(z) = \frac{Y_h(z)z^{-1}}{1+Y_h(z)C(z)z^{-2}} \quad (8)$$

And obtaining the forward path transfer function of the system:

$$FW(z) = -CC_{loop}(z)z^{-1} \quad (9)$$

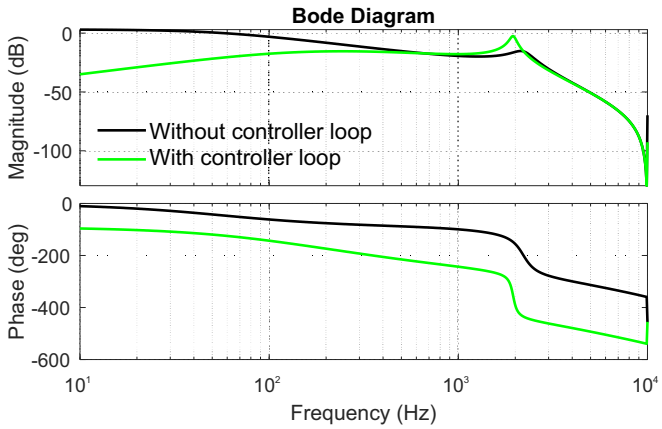

FIGURE 4. **The impact of the controller loop on the PHIL analysis transfer function $\frac{I_h(z)}{V^*(z)}$.**

The closed-loop transfer function for the PHIL system $\frac{I_h(z)}{V^*(z)}$ is finally obtained:

$$\frac{I_h(z)}{V^*(z)} = \frac{FW(z)}{1 - FW(z)Z_s(z)F(z)z^{-1}} \tag{10}$$

As can be noted, the transfer function $\frac{I_h(z)}{V^*(z)}$ in the classical (5) and in the proposed analysis (10) approach differ substantially. To illustrate this difference, in Fig. 4, the Bode diagrams of the two transfer functions is shown when the current controller proportional gain is $K_p = 8$ and a filter with a time constant $T_f = 300\,\mu$s is used.

As depicted in the figure, the frequency behavior between the classical model without modeling the converter control for PHIL stability analysis and the proposed model, which includes the converter controller model, has apparent differences. At lower frequencies, the classical approach overestimates the frequency amplitude, while at higher frequencies, it underestimates the resonance peak. Also, the frequency of resonance appears to be lower due to the current controller. Furthermore, the phase diagram shows an entirely different behavior in the frequency spectrum, which may lead to an incorrect assessment of the gain and phase margin during the loop stability analysis.

The transfer function $\frac{I_h(z)}{I^*(z)}$, which involves the capability of the converter to follow its reference, can be determined considering the open-loop and PHIL closed-loop transfer function:

$$H_{loop}(z) = F(z)Z_s(z)z^{-1} \tag{11}$$

$$CH_{loop}(z) = \frac{Y_h(z)z^{-1}}{1 + Y_h(z)H_{loop}(z)z^{-1}} \tag{12}$$

From this point, the converter transfer function $\frac{I_h(z)}{I^*(z)}$ can be determined as in (13):

$$\frac{I_h(z)}{I^*(z)} = \frac{C(z)CH_{loop}(z)}{1 + C(z)CH_{loop}(z)z^{-1}} \tag{13}$$

TABLE 2. **PHIL simulation parameters.**

T_s [μs]	T_d [μs]	T_f [μs]	R_s [Ω]	L_s [mH]	L_g [mH]	L_c [mH]	C_f [μF]	R_f, R_g [Ω]	R_c [Ω]	Kp —	Ki —
50	50	50	0.5	0.31	0.93	0.85	10	0.1	2	5.59	628.31

TABLE 3. **Verification of the PHIL Transfer Function, $\frac{I_h(z)}{V^*(z)}$.**

Frequency (Hz)	Transfer Function	Simulink	Parameter
100	1.33	1.33	Gain (absolute)
	-143	-142	Phase (Degree)
150	1.57	1.58	Gain (absolute)
	-160	-159	Phase (Degree)
200	1.67	1.67	Gain (absolute)
	-173	-173	Phase (Degree)
300	1.67	1.675	Gain (absolute)
	167	168	Phase (Degree)
500	1.49	1.41	Gain (absolute)
	144	145	Phase (Degree)
700	1.35	1.17	Gain (absolute)
	131	131	Phase (Degree)
850	1.01	1.29	Gain (absolute)
	123	123	Phase (Degree)
1000	1.28	0.86	Gain (absolute)
	116	116	Phase (Degree)

This transfer function will be particularly important in the next section to compare the converter frequency behavior in the naturally-coupled and the PHIL-coupled system.

IV. VERIFICATION OF THE TRANSFER FUNCTIONS

The calculated closed-loop transfer functions of the PHIL and the converter from the previous section are verified using MATLAB/Simulink. The PHIL described in Fig. 2 (without feedforward) is implemented in Simulink using the parameters given in Table 2. Different sample frequencies via perturbation sources are applied to the system, namely V_p to verify the PHIL closed-loop transfer function and I_p to confirm the converter transfer function. Then, I_h is measured and fed into the Fourier block to obtain the gains and phases at each frequency. These measured values are compared to the frequency response of the obtained transfer functions in Table 3 and Table 4, respectively.

By comparing the transfer function frequency response and the measured values from the Fourier block in Simulink,

TABLE 4. Verification of the Converter Transfer Function, $\frac{I_h(z)}{I^*(z)}$.

Frequency (Hz)	Transfer Function	Simulink	Parameter
100	1.04	1.04	Gain (absolute)
	-10	-10	Phase (Degree)
150	1.05	1.04	Gain (absolute)
	-17	-17	Phase (Degree)
200	1.03	1.03	Gain (absolute)
	-24	-24	Phase (Degree)
300	0.97	0.97	Gain (absolute)
	-36	-36	Phase (Degree)
500	0.85	0.83	Gain (absolute)
	-55	–55	Phase (Degree)
700	0.75	0.77	Gain (absolute)
	-69	-70	Phase (Degree)
850	0.71	0.74	Gain (absolute)
	-78	-80	Phase (Degree)
1000	0.70	0.74	Gain (absolute)
	-86	-90	Phase (Degree)

it can be seen that the gain and phase values are nearly equal at each sample frequency. From the tables, the correctness of the calculated transfer functions to describe the dynamic behavior of the benchmark can be concluded.

V. IMPACT OF HOI ON PHIL EVALUATION

This section aims to demonstrate the effect of different current controllers' bandwidths on the stability and accuracy of the PHIL evaluation.

To assess the influence of different controller bandwidths, the current controller bandwidth is varied between [100–1100] Hz in both the naturally-coupled and PHIL-coupled systems. The grid impedance is $Z_s = 1 + j0.2\ \Omega$ and the low-pass filter bandwidth is 150 μs. The objective is to observe how the PHIL transfer function changes with bandwidth and how closely it matches the behavior of the naturally-coupled system. The PZ map of the converter loop, $\frac{I_h(z)}{I^*(z)}$, and PHIL $\frac{I_h(z)}{V^*(z)}$, is presented in Fig. 5 and Fig. 6, respectively.

As can be noted, the naturally-coupled system behaves differently from the PHIL system. While the naturally-coupled system remains stable with a current controller bandwidth of 900 Hz, the PHIL system is already unstable at 500 Hz. To prove that, the time domain responses of the closed-loop system are depicted in Fig. 7 and Fig. 8 at a controller bandwidth of 700 Hz, confirming the pole-zero map outputs.

Also, by looking at the Bode plot in Fig. 9, it can be noted that the PHIL is able to represent accurately the system up to 2 kHz at low bandwidths (e.g., 100 Hz). However, the accuracy deteriorates as the current controller bandwidth increases. As an example, for the bandwidth of 500 Hz, the two frequency responses begin to differ above the 1 kHz threshold. The deviation can be seen even before 1000 Hz when the bandwidth is close to 1.1 kHz. This indicates that at higher frequencies, the HoI no longer behaves as in the real field, invalidating the purpose of the PHIL evaluation.

If we look at the Bode plot of the transfer function $\frac{I_h(z)}{V^*(z)}$, shown in Fig. 10, it can be noted that there is a worse noise rejection capability from the PHIL system with the increase in the current controller bandwidth. This implies that any external noise will be amplified under high converter bandwidths.

VI. IMPACT OF THE FEEDBACK FILTER

In this section, the interface feedback filter is designed to guarantee sufficient stability in large operation points.

A feedback filter typically has a stabilizing effect, allowing otherwise unstable systems to regain stability. In Fig. 11 and Fig. 12 the poles of the transfer function $\frac{I_h(z)}{I^*(z)}$, and $\frac{I_h(z)}{V^*(z)}$ are plotted, considering a current controller bandwidth of 700 Hz and a system impedance of $Z_s = 1 + j0.2\ \Omega$. It can be seen that a feedback filter of only 550 μs (i.e., 1820 Hz) can let the system regain stability.

However, this comes at a price in terms of accuracy along the frequency spectrum. As can be noted in Fig. 13, the slower the used filter, the larger the difference between the frequency response of the naturally-coupled and PHIL systems. In the case of a slow filter (e.g., $>$ 500 μs), signals

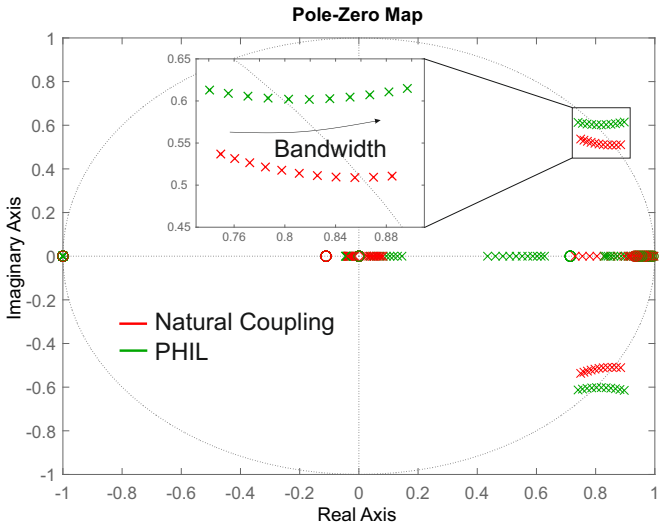

FIGURE 5. Poles of the transfer function $\frac{I_h(z)}{I^*(z)}$, considering variable current controller bandwidth (100 Hz to 1.1 kHz).

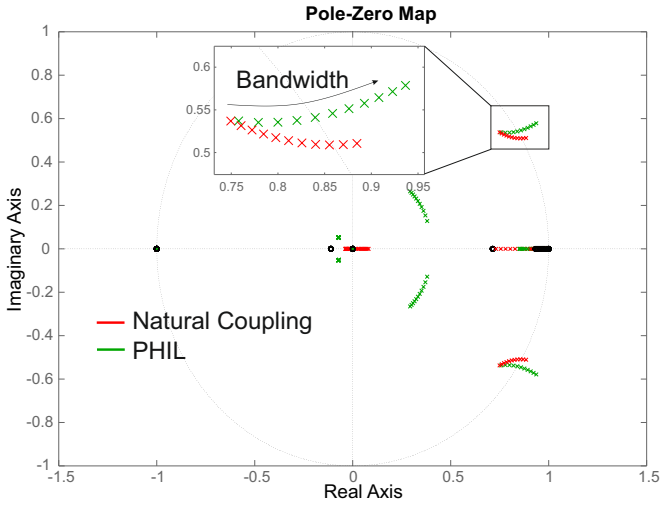

FIGURE 6. Poles of the transfer function $\frac{I_h(z)}{V^*(z)}$, considering variable current controller bandwidth (100 Hz to 1.1 kHz).

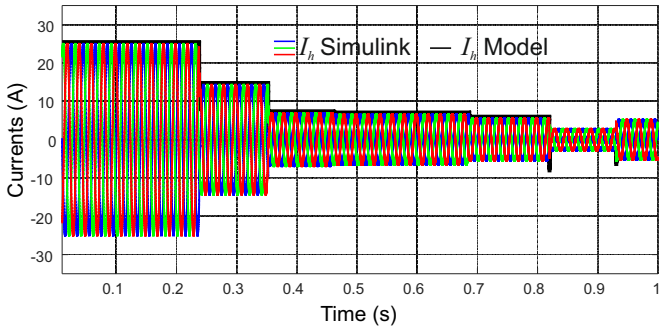

FIGURE 7. Time response of the natural coupling at controller bandwidth 700 Hz.

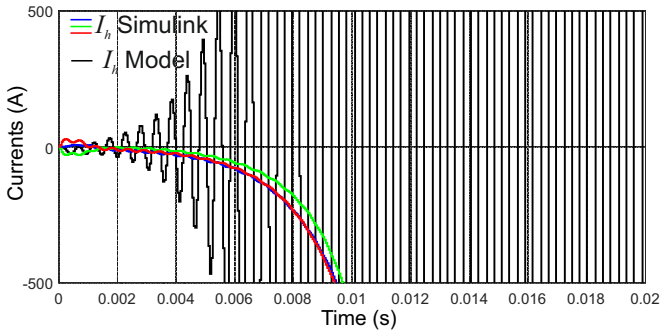

FIGURE 8. Time response of the PHIL at controller bandwidth 700 Hz.

above 1 kHz are damped, and the resonance peak of the LCL filter is shifted to higher frequencies.

VII. IMPACT OF SIMULATED GRID IMPEDANCE

One of the main uncertainties of the PHIL evaluation is the complex value of the grid impedance Z_s. The grid impedance changes depending on the connected loads and generators, namely the grid configuration, which leads to changes to the Thevenin equivalent. To achieve a stable PHIL evaluation, the impact of impedance values under different feedback

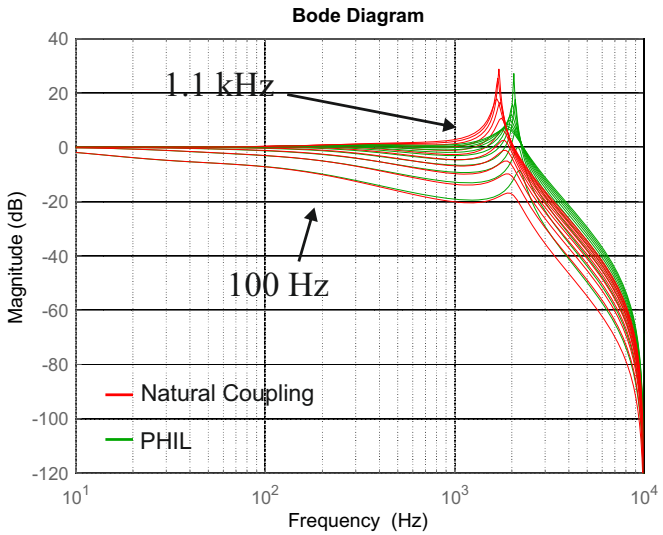

FIGURE 9. Bode plot of the transfer function $\frac{I_h(z)}{I^*(z)}$, considering variable current controller bandwidth (100 Hz to 1.1 kHz).

filter gains can be evaluated prior to conducting experiments.

For each of the five different values of Z_s, as demonstrated in Fig. 14, the time constant of the filter is varied from T_s to 11 times of it. It can be concluded that, to regain the stability of the PHIL against changes in the grid impedance, the time constant of the filter can be accordingly changed; however, as discussed above, the high time constant of the filter deteriorates the accuracy of the PHIL.

VIII. EXPERIMENTAL RESULTS

To validate the PHIL and the converter models achieved in section III, a PHIL setup at the Karlsruhe Institute of Technology has been employed, with a grid emulator as a Real-Time Digital Simulator (RTDS) system and three APS 15000 4-quadrant linear amplifiers from Spitzenberger

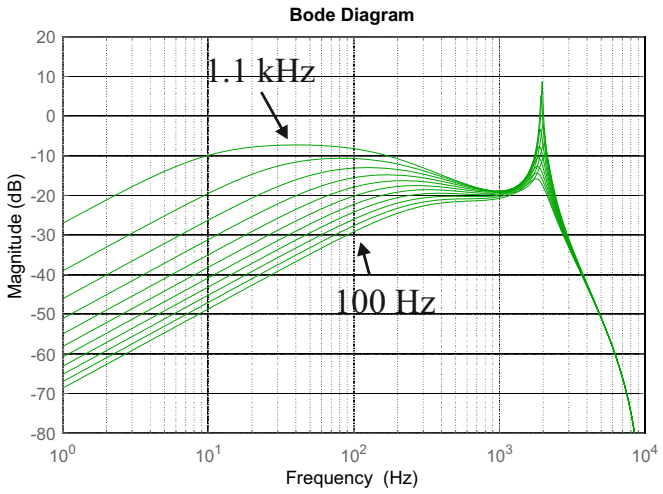

FIGURE 10. Bode plot of the transfer function $\frac{I_h(z)}{V^*(z)}$, considering variable current controller bandwidth (100 Hz to 1.1 kHz).

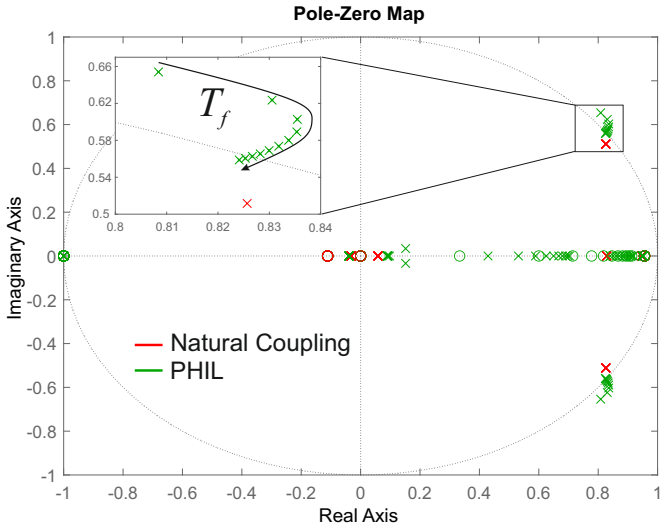

FIGURE 11. **Poles of the transfer function $\frac{I_h(z)}{I^*(z)}$, considering different filter time constants [$50\ \mu s - 550\ \mu s$].**

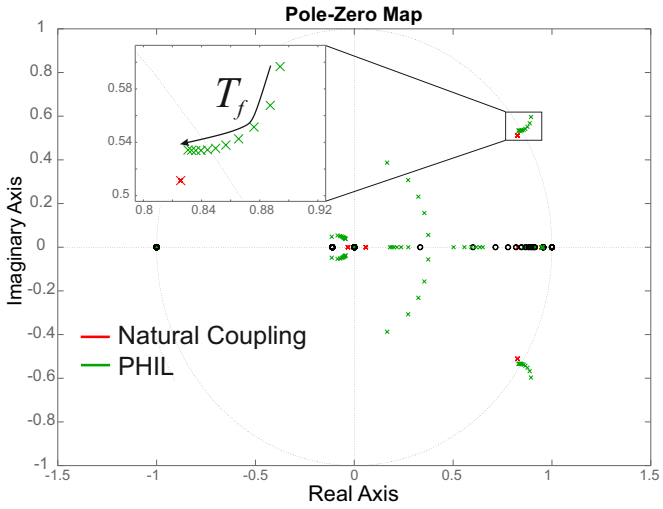

FIGURE 12. **Poles of the transfer function $\frac{I_h(z)}{V^*(z)}$, considering different filter time constants [$50\ \mu s - 550\ \mu s$].**

& Spies, as shown in Fig. 15. Three PEB8038 half-bridge modules, a B-Box RCP digital controller, LCL filters from Imperix, and an EA-PSI 91500-30 WR 3U DC supply constitute a 3-phase DC/AC converter as the HoI. Parameter values for the experiment are given in Table 5. Thevenin model of the grid is implemented in RSCAD with a series RL load, namely R_s and L_s. T_s is the time step of the RTDS, and consequently, the loop delay coming from the real-time simulator becomes two times T_s, i.e., one T_s in forward and one in the feedback shown as T_{DRTS}.

A low-pass filter is used in RSCAD with a cut-off frequency of 2 kHz to reject high-frequency measurement noises. The delay of the amplifier, including the D/A conversion, using the Small Form-factor Pluggable (SFP) connection is T_{conv}. L_f, L_g, and C_f are the passive filter parameters where R_f, and R_g are the resistive part of inductor and R_c is that of capacitor. The current controller

TABLE 5. **PHIL experiment parameters.**

T_s [μs]	T_{DRTS} [μs]	T_{conv} [μs]	R_s [Ω]	L_s [mH]	L_c, L_g [mH]	C_f [μF]	R_f, R_g [Ω]	R_c [Ω]	Kp —	Ki —
50	100	4.1	0.005	0.22	2.5	12	0.045	1.5	0.1	40

is a PI whose parameters are shown as K_p proportional gain and K_i integral gain. A frequency scan is performed on the described setup in two cases. In the first case, perturbation i_p, with the frequency range of [100-1000] Hz (f_p) and the magnitude of 55 A, is added to the reference current of the PI controller, I^*, and the corresponding harmonic is measured at the PCC, I_h, using DIN RAIL-MOUNTABLE current sensors of Imperix. The current signal, denoted as I^*, and the measured current signal, referred to as I_h, are fed into the Fourier block within the MATLAB/Simulink environment. This specific step is essential for computing the gain and phase of the ratio I_h/I^* at each harmonic frequency. The resulting outcomes, presented as red stars, are then compared with the results obtained through the model implemented in Simulink, as illustrated in Fig. 16.

The same procedure is taken for verification of I_h/V^*. This time, perturbations are added to the voltage source in RTDS, V_p, with a magnitude of 20 V, and the current is measured with the amplifiers' current sensors, IT 700-S ULTRASTAB. The measured gain and phase comparison is shown in Fig. 17. In both cases, the close agreement between the measured frequency response and the simulation results serves as evidence confirming the validity of the obtained transfer functions.

In addition to Bode plots, a quantitative assessment is performed to evaluate the validity of the modeled transfer functions across measured gains and phases from experiments, using the normalized root-mean-square error (nRMSE) and maximum deviation error (MaxDev). The following equa-

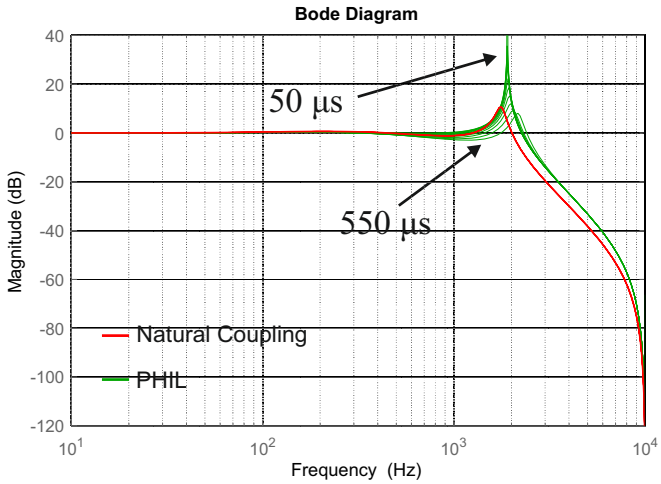

FIGURE 13. **Filter impact from Ts to 11*Ts with respect to the natural coupling.**

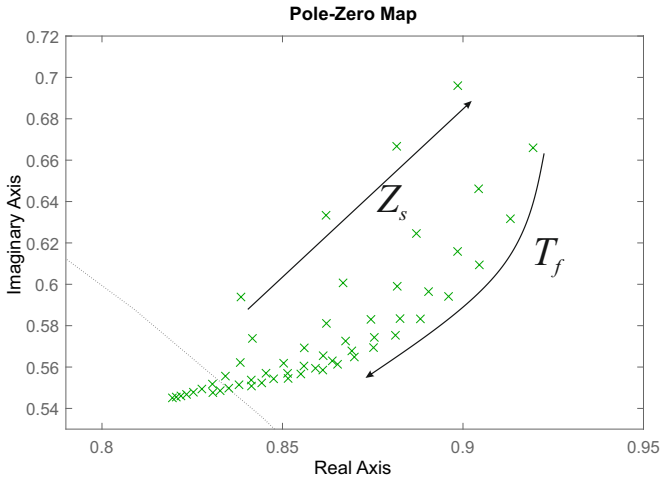

FIGURE 14. Filter impact from Ts to 11*Ts vs. grid impedance's resistance impact from 0.5 to 50 Ω for current controller bandwidth of 700 Hz.

tions are used to achieve these error metrics:

$$\text{RMSE}_{\text{gain}} = \sqrt{\frac{1}{N}\sum_{i=1}^{N}\left(|CL_{model}(j\omega_i)| - |CL_{exp}(j\omega_i)|\right)^2} \tag{14}$$

$$\text{RMSE}_{\text{phase}} = \sqrt{\frac{1}{N}\sum_{i=1}^{N}\left(\angle CL_{model}(j\omega_i) - \angle CL_{exp}(j\omega_i)\right)^2} \tag{15}$$

Where $|CL_{exp}(j\omega)|$ and $|CL_{model}(j\omega)|$ are the measured gain of the closed-loop transfer function (I/I^* or I/V^*) from experiments and modeling, respectively. The symbol $\angle$ represents the phase, i is the perturbation number, and N is the number of perturbation samples, i.e., 9 (from 200 to 1000 with a step of 100). The RMSE is then normalized by the range of experimentally measured values using the following equation:

$$\text{nRMSE} = \frac{\text{RMSE}}{\max_i\{CL_{exp}(j\omega_i)\} - \min_i\{CL_{exp}(j\omega_i)\}} \tag{16}$$

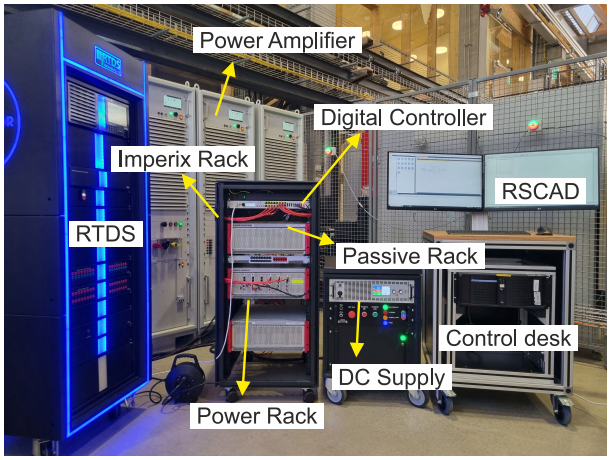

FIGURE 15. PHIL setup realized at the Energy Lab 2.0.

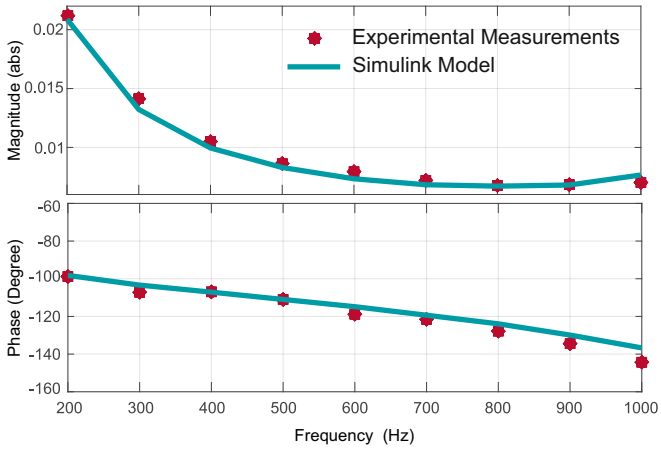

FIGURE 16. Frequency response comparison of $\frac{I_h}{I^*}$.

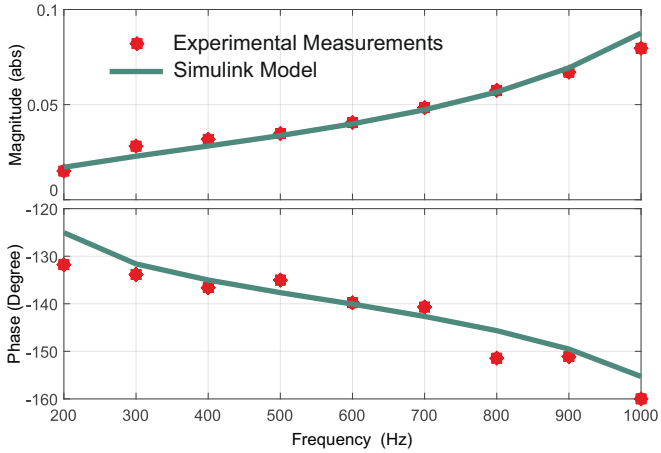

FIGURE 17. Frequency response comparison of $\frac{I_h}{V^*}$.

TABLE 6. Accuracy of the modeling based on experiments.

Closed-Loop / Error Index	I_h/I^*		I_h/V^*	
	Gain	Phase	Gain	Phase
nRMSE	0.055	0.036	0.080	0.025
MaxDev	0.001	8.942	0.007	6.747

The equations used to evaluate MaxDev are:

$$\text{MaxDev}_{\text{gain}} = \max_i\left||CL_{exp}|(j\omega_i) - |CL_{model}(j\omega_i)|\right| \tag{17}$$

$$\text{MaxDev}_{\text{phase}} = \max_i\left|\angle CL_{exp}(j\omega_i) - \angle CL_{model}(j\omega_i)\right| \tag{18}$$

Applying the measured values of gain and phase from each closed-loop transfer function to the equations described above will result in Table 6. From the Bode plots and the output results of the Table 6, the validity of the modeling of the benchmark PHIL, and the achieved transfer functions can be concluded.

IX. CONCLUSION

Developing power-electronics-dominated electrical grids necessitates accurate and reliable testing methodologies. Power

Hardware-in-the-loop (PHIL) has emerged as a key approach for realistically simulating grid behavior to test the system-level power electronic technologies. However, the stability and accuracy of PHIL setups are often constrained by a trade-off, primarily due to the effects introduced by the interface components. This paper investigates the influence of not only the interface components but also an active Hardware-of-Interest (HoI) on the PHIL stability and accuracy. It is shown that the current controller bandwidth of a three-phase grid-following converter as a HoI affects the accuracy of PHIL results. The analysis is conducted by modeling the three main components of a PHIL system—the Model of Interest (MoI), the interface, and the HoI—using their respective transfer functions. These transfer functions are validated through perturbation-based simulations in Simulink. Subsequently, the sensitivity of PHIL stability and accuracy to both the current controller bandwidth and the interface feedback filter is evaluated. The results indicate that the choice of current controller parameters not only affects PHIL stability but also significantly influences accuracy, indicating the need for a more conservative controller tuning and a more refined feedback filter design. To further validate the findings, the derived transfer functions are experimentally verified using a 45 kVA PHIL setup incorporating an Imperix PEB8038 converter.

REFERENCES

[1] F. Blaabjerg, R. Teodorescu, M. Liserre, and A. Timbus, "Overview of control and grid synchronization for distributed power generation systems," *IEEE Transactions on Industrial Electronics*, vol. 53, no. 5, pp. 1398–1409, 2006.

[2] A. Helmedag, T. Isermann, A. Monti, N. R. Averous, M. Stieneker, and R. W. De Doncker, "Multi-physics power hardware in the loop test bench for on-shore wind turbine nacelles," in *2013 IEEE ECCE Asia Downunder*, pp. 221–226, 2013.

[3] K. Moslehi and R. Kumar, "A reliability perspective of the smart grid," *IEEE Transactions on Smart Grid*, vol. 1, no. 1, pp. 57–64, 2010.

[4] A. Benigni, T. Strasser, G. De Carne, M. Liserre, M. Cupelli, and A. Monti, "Real-time simulation-based testing of modern energy systems: A review and discussion," *IEEE Industrial Electronics Magazine*, vol. 14, no. 2, pp. 28–39, 2020.

[5] G. F. Lauss, M. O. Faruque, K. Schoder, C. Dufour, A. Viehweider, and J. Langston, "Characteristics and design of power hardware-in-the-loop simulations for electrical power systems," *IEEE Transactions on Industrial Electronics*, vol. 63, no. 1, pp. 406–417, 2016.

[6] C. S. Edrington, M. Steurer, J. Langston, T. El-Mezyani, and K. Schoder, "Role of power hardware in the loop in modeling and simulation for experimentation in power and energy systems," *Proceedings of the IEEE*, vol. 103, no. 12, pp. 2401–2409, 2015.

[7] F. Huerta, J. K. Gruber, M. Prodanovic, and P. Matatagui, "Power-hardware-in-the-loop test beds: evaluation tools for grid integration of distributed energy resources," *IEEE Industry Applications Magazine*, vol. 22, no. 2, pp. 18–26, 2016.

[8] S. D'Arco, S. Sanchez-Acevedo, and J. A. Suul, "Multi-hardware-in-the-loop laboratory testing of power converters and intelligent electronic devices for large-scale power system applications," *IEEE Open Journal of Power Electronics*, vol. 5, pp. 1520–1533, 2024.

[9] O. Tremblay, H. Fortin-Blanchette, R. Gagnon, and Y. Brissette, "Contribution to stability analysis of power hardware-in-the-loop simulators," *IET Generation, Transmission & Distribution*, vol. 11, no. 12, pp. 3073–3079, 2017.

[10] W. Ren, M. Steurer, and T. L. Baldwin, "Improve the stability and the accuracy of power hardware-in-the-loop simulation by selecting appropriate interface algorithms," *IEEE Transactions on Industry Applications*, vol. 44, no. 4, pp. 1286–1294, 2008.

[11] G. Lauss and K. Strunz, "Accurate and stable hardware-in-the-loop (hil) real-time simulation of integrated power electronics and power systems," *IEEE Transactions on Power Electronics*, vol. 36, no. 9, pp. 10920–10932, 2021.

[12] F. Ashrafidehkordi, X. Liu, and G. De Carne, "Impedance-based stability analysis of a power hardware-in-the-loop for grid-following inverter testing," in *2023 IEEE Energy Conversion Congress and Exposition (ECCE)*, pp. 1116–1121, 2023.

[13] S. Okumu, F. Ashrafidehkordi, and G. De Carne, "Source impact of a dc/ac converter on impedance-based stability analysis for power hardware-in-the-loop setups," in *2024 9th IEEE Workshop on the Electronic Grid (eGRID)*, pp. 1–5, 2024.

[14] M. U. Rafiq, S. Pugliese, and M. Liserre, "Modeling of symmetrical and asymmetrical grid faults for p-hil accuracy analysis in lvrt tests," in *2022 IEEE Energy Conversion Congress and Exposition (ECCE)*, pp. 1–8, 2022.

[15] E. Guillo-Sansano, M. H. Syed, A. J. Roscoe, G. M. Burt, and F. Coffele, "Characterization of time delay in power hardware in the loop setups," *IEEE Transactions on Industrial Electronics*, vol. 68, no. 3, pp. 2703–2713, 2021.

[16] M. Davari, O. Qasem, W. Gao, F. Blaabjerg, P. C. Kotsampopoulos, G. Lauss, and N. D. Hatziargyriou, "A reinforcement-learning, optimal approach to in situ power hardware-in-the-loop interface control for testing inverter-based resources: Theory and application of the adaptive dynamic programming based on the hybrid iteration to tackle uncertain dynamics," *IEEE Transactions on Industrial Electronics*, vol. 72, no. 6, pp. 5867–5883, 2025.

[17] M. Pokharel and C. N. M. Ho, "Development of interface model and design of compensator to overcome delay response in a phil setup for evaluating a grid-connected power electronic dut," *IEEE Transactions on Industry Applications*, vol. 58, no. 3, pp. 4109–4121, 2022.

[18] J. Constantine, K. L. Lian, Y. F. Fan, C. Y. Xiao, and Z.-P. He, "New power interface based on multi-dimensional golden section search algorithm for power-hardware-in-the-loop applications," *IEEE Access*, vol. 12, pp. 14487–14498, 2024.

[19] S. Chakraborty, M. T. Rana, and M. V. Salapaka, "A robust power hardware-in-the-loop interface under uncertain software and hardware system," *IEEE Transactions on Industrial Electronics*, vol. 72, no. 6, pp. 6088–6102, 2025.

[20] J. K. Banda, D. D. S. Mota, and E. Tedeschi, "A physics-informed scaling method for power electronic converters in power hardware-in-the-loop test beds," *IEEE Open Journal of Industry Applications*, vol. 5, pp. 1–14, 2024.

[21] Q. Lin, B. Wen, and R. Burgos, "Rhp poles trajectory study for d–q impedance-based stability monitoring using a power-hardware-in-the-loop testbed," *IEEE Journal of Emerging and Selected Topics in Power Electronics*, vol. 12, no. 2, pp. 1560–1572, 2024.

[22] K. Prabakar, B. Palmintier, A. Pratt, A. Hariri, I. Mendoza, and M. Baggu, "Improving the performance of integrated power-hardware-in-the-loop and quasi-static time-series simulations," *IEEE Transactions on Industrial Electronics*, vol. 68, no. 11, pp. 10938–10948, 2021.

[23] I. D. Yoo and A. M. Gole, "Compensating for interface equipment limitations to improve simulation accuracy of real-time power hardware in loop simulation," *IEEE Transactions on Power Delivery*, vol. 27, no. 3, pp. 1284–1291, 2012.

[24] T. Hatakeyama, A. Riccobono, and A. Monti, "Stability and accuracy analysis of power hardware in the loop system with different interface algorithms," in *2016 IEEE 17th Workshop on Control and Modeling for Power Electronics (COMPEL)*, pp. 1–8, 2016.

[25] J. Siegers and E. Santi, "Improved power hardware-in-the-loop interface algorithm using wideband system identification," in *2014 IEEE Applied Power Electronics Conference and Exposition - APEC 2014*, pp. 1198–1204, 2014.

[26] A. Riccobono, E. Liegmann, M. Pau, F. Ponci, and A. Monti, "Online parametric identification of power impedances to improve stability and accuracy of power hardware-in-the-loop simulations," *IEEE Transactions on Instrumentation and Measurement*, vol. 66, no. 9, pp. 2247–2257, 2017.

[27] S. Paran and C. S. Edrington, "Improved power hardware in the loop interface methods via impedance matching," in *2013 IEEE Electric Ship Technologies Symposium (ESTS)*, pp. 342–346, 2013.

[28] G. Lauss, F. Lehfuss, A. Viehweider, and T. Strasser, "Power hardware in the loop simulation with feedback current filtering for electric

systems," in *IECON 2011 - 37th Annual Conference of the IEEE Industrial Electronics Society*, pp. 3725–3730, 2011.
[29] Z. Feng, R. Pena-Alzola, P. Seisopoulos, E. Guillo-Sansano, M. Syed, P. Norman, and G. Burt, "A scheme to improve the stability and accuracy of power hardware-in-the-loop simulation," in *IECON 2020 The 46th Annual Conference of the IEEE Industrial Electronics Society*, pp. 5027–5032, 2020.
[30] W. Ren, M. Steurer, and T. L. Baldwin, "An effective method for evaluating the accuracy of power hardware-in-the-loop simulations," *IEEE Transactions on Industry Applications*, vol. 45, no. 4, pp. 1484–1490, 2009.
[31] O. Tremblay, H. Fortin-Blanchette, R. Gagnon, and Y. Brissette, "Contribution to stability analysis of power hardware-in-the-loop simulators," *IET Generation, Transmission Distribution*, vol. 11, no. 12, pp. 3073–3079, 2017.
[32] F. Ashrafidehkordi, D. Kottonau, and G. De Carne, "Multi-rate discrete domain modeling of power hardware-in-the-loop setups," *IEEE Open Journal of Power Electronics*, vol. 4, pp. 539–548, 2023.
[33] D. D. S. Mota, J. K. Banda, A. A. Adeyemo, and E. Tedeschi, "Harmonic-invariant scaling method for power electronic converters in power hardware-in-the-loop test beds," *IEEE Open Journal of Industry Applications*, vol. 4, pp. 139–148, 2023.
[34] G. De Carne, M. Langwasser, M. Ndreko, R. Bachmann, R. W. De Doncker, R. Dimitrovski, B. J. Mortimer, A. Neufeld, F. Rojas, and M. Liserre, "Which deepness class is suited for modeling power electronics?: A guide for choosing the right model for grid-integration studies," *IEEE Industrial Electronics Magazine*, vol. 13, no. 2, pp. 41–55, 2019.
[35] C. Zhang, G. Buticchi, J. Yang, and Z. Zou, "Control and stabilization of grid-connected converters operating as constant power load in a smart transformer grid scenario," in *IECON 2020 The 46th Annual Conference of the IEEE Industrial Electronics Society*, pp. 2895–2900, 2020.

Fargah Ashrafidehkordi (Student Member, IEEE) received the B.Sc. and M.Sc. degrees in electrical engineering from Babol Noshirvani University of Technology, Iran, in 2016, and Amirkabir University of Technology, Iran, in 2019, respectively. He is currently pursuing the Ph.D. degree at the Karlsruhe Institute of Technology (KIT), Germany, where he is a senior member of the "Real Time Systems for Energy Technologies" group of the Institute for Technical Physics (ITEP). His research focuses on the stability and modeling of Power Hardware-in-the-Loop (PHIL) systems. His interests include power electronics integration in power systems, control and protection of grid converters, smart transformers, impedance-based modeling, and stability analysis.

Giampaolo Buticchi (S'10-M'13-SM'17) received the Master degree in Electronic Engineering in 2009 and the Ph.D degree in Information Technologies in 2013 from the University of Parma, Italy. Between 2014 and 2017, he was a post-doctoral researcher and Guest Professor at the University of Kiel, Germany. He was appointed as an Associate Professor at The University of Nottingham Ningbo China in 2017 and promoted to Professor in 2020. He is now the Head of the Power Electronics, Machine and Control Research Centre at his institution. His research focuses on power electronics for renewable energy systems, smart transformer fed micro-grids, and dc grids for transportation applications. Dr. Buticchi is involved in the major international organizations (IEEE, IET, RAeS, HEA), and he is a Co-Editor in Chief of the IEEE Transactions on Industrial Electronics and the Recipient of the IEEE-IES David J. Irwin Early Career Award.

Panos Kotsampopoulos received the Diploma in Electrical and Computer Engineering and his PhD degree from NTUA in 2010 and 2017, respectively. Since 2009, he has been a member of the Smart RUE research group at ICCS-NTUA and is now a Principal Researcher at ICCS in the field of Smart Grids and Adjunct Lecturer at ECE-NTUA. He was a guest researcher at the Austrian Institute of Technology (AIT) in 2012 and 2013. He coordinated the H2020 RE-EMPOWERED (Renewable Energy Empowering European & Indian Communities) project. He is secretary-elect of the University Education Activities Subcommittee of IEEE PES PEEC and treasurer of the IEEE Greece PES Chapter. He is chair of the IEEE PES Task Force "Innovative teaching methods for modern power and energy systems", chapter leader of IEEE WG P2004, past chair of IEEE Young Professionals Greece, and member of the Editorial Board of the "IEEE Open Access Journal of Power and Energy" and the journal "Energies". He is the co-founder of the energy community "Collective Energy" (COEN). He is a Senior Member of IEEE and a recipient of the 2020 best paper award of the IEEE Open Access Journal of Power and Energy.

Giovanni De Carne (Senior Member, IEEE) received the B.Sc. and M.Sc. degrees in electrical engineering from the Polytechnic University of Bari, Italy, in 2011 and 2013, respectively, and the Ph.D. degree from the Chair of Power Electronics, Kiel University, Germany, in 2018. Prof. De Carne is currently W3 (full) professor at the Institute for Technical Physics at the Karlsruhe Institute of Technology, Karlsruhe, Germany, where he leads the "Real Time Systems for Energy Technologies" Group and the "Power Hardware In the Loop Lab". He is currently supervising PhD students, managing academic and industrial projects, and developing multi-MW power hardware in the loop testing infrastructures for energy storage systems and hydrogen-based drives. He has authored/co-authored more than 100 peer-reviewed scientific papers. His research interests include power electronics integration in power systems, solid-state transformers, real-time modelling, and power hardware in the loop. Prof. De Carne successfully hosted the IEEE eGrid2023 Workshop in Karlsruhe in October 2023 with high participation from the industry. He has been the technical program committee chair for several IEEE conferences, and associate editor of the IEEE Open Journal of Power Electronics and several other IEEE and IET journals.